EUROPEAN ORGANIZATION FOR NUCLEAR RESEARCH

CERN-PPE/91-28
5 February 1991

OBSERVATION OF A 2^{++} RESONANCE AT 1515 MeV IN PROTON ANTIPROTON ANNIHILATIONS INTO $3\pi^0$

The Crystal Barrel Collaboration

E. Aker[12], C. Amsler[12], I. Augustin[5], C.A. Baker[10], B.M. Barnett[12], C.J. Batty[10], R. Beckmann[3], P. Birien[1], J. Bistirlich[1], P. Blüm[5], R. Bossingham[1], H. Bossy[1], K. Braune[9], M. Burchell[2], T. Case[1], S. Cierjacks[4], K.M. Crowe[1], K. Dederichs[9], W. Dünnweber[9], D. Engelhardt[5], M.A. Faessler[9], C. Felix[9], G. Folger[9], R. Haddock[7], F.H. Heinsius[3], N.P. Hessey[10], P. Hidas[2], P. Illinger[9], D. Jamnik[9+], H. Kalinowsky[8], B. Kämmle[3], T. Kiel[3], E. Klempt[8], H. Koch[5,a], K. Königsmann[9], M. Kunze[5,a], R. Landua[2], B. Lewendel[3], H. Matthaey[5], M. Merkel[8], C.A. Meyer[12], U. Meyer-Berkhout[9], L. Montanet[2], C. Pegel[3], K. Peters[8]*, S. Ravndal[5,a], A.H. Sanjari[6], E. Schäfer[8], B. Schmid[12], W. Schott[5], U. Strohbusch[3], M. Suffert[11], C. Sutton[5], D. Urner[12], D. Walther[2], S. Walther[8], U. Wiedner[3,8], N. Winter[5], J. Zoll[2], and C. Zupancic[9]

1 University of California, Lawrence Berkeley Laboratory, CA 94720, USA.
2 CERN, CH-1211 Geneva 23, Switzerland.
3 Universität Hamburg, D-2000 Hamburg, Germany.
4 Institut für Material und Festkkörperforschung, Kernforschungszentrum Karlsruhe, D-7500 Karlsruhe, Germany.
5 Universität Karlsruhe, D-7500 Karlsruhe, Germany.
6 Queen Mary and Westfield College, London E1 4NS, UK.
7 University of California, Los Angeles, CA 90024, USA.
8 Universität Mainz, D-6500 Mainz, Germany.
9 Universität München, D-8000 München, Germany.
10 Rutherford Appleton Laboratory, Chilton, Didcot OX11 0QX, UK.
11 Centre de Recherches Nucléaires, F-67037 Strasbourg, France.
12 Universität Zürich, CH-8001 Zürich, Switzerland.

* The analysis presented here is part of the Ph.D. thesis of K. Peters.
+ On leave of absence from the University of Ljubljana, Yugoslavia.
a Present address: Universität Bochum, D-4630 Bochum, Germany.

ABSTRACT

Antiproton-proton annihilations at rest into $3\pi^o$ are analyzed in terms of $\pi^o\pi^o$ final state interactions. A $J^{PC} = 2^{++}$ resonance at a mass of (1515 ± 10) MeV with a width of (120 ± 10) MeV is required to explain the data. This result is supported by previous observations made on the $\pi\pi$ system in $\bar{p}p$ and $\bar{p}n$ annihilations which show that the resonance has I = 0. This resonance is practically degenerate in mass with the f_2' (1525) but the two resonances have very different production and decay characteristics.

Annihilations of antiprotons stopped in liquid hydrogen and deuterium targets have been studied for more than twenty years. One of the first detailed analyses of the $\pi^+\pi^-\pi^o$ channel [1] revealed the dominance of the process:

$$^{13}S_1(\bar{p}p) \rightarrow \rho(770)\pi \rightarrow \pi^+\pi^-\pi^o .$$

The analysis of $\bar{p}n \rightarrow \pi^-\pi^-\pi^+$ [2] and of $\bar{p}p \rightarrow 3\pi^o$ annihilations [3] revealed new features which triggered much theoretical interest in the hey-days of dual models [4]. However, it was soon recognized [5] that dual models cannot provide a good quantitative explanation of the data without an unpalatable number of arbitrary parameters. Meanwhile, a new approach was tried, in which P states of the initial nucleon-antinucleon pair were also considered [6], and it was demonstrated [7] that all three pion annihilations could then be explained by the dominance of intermediate resonances provided that a new isoscalar two-pion resonance of positive parity was postulated at 1527 MeV. On the basis of weak arguments, it was "cautiously suggested" [7] that the spin of the new resonance is zero. This pioneer work showed that more precise information on P wave $\bar{p}p$ annihilations and on $\bar{p}p \rightarrow 3\pi^o$ [where the $\rho(770)$ is absent] would be welcome.

At the CERN Low Energy Antiproton Ring (LEAR), the ASTERIX Collaboration, studying the annihilation of antiprotons stopped in hydrogen gas, isolated annihilations from P states and found that a new resonance at 1565 MeV with isospin zero and spin J = 2 was present in P state $\bar{p}p$ annihilations into $\pi^+\pi^-\pi^o$ [8]. Taking into account the various limitations and uncertainties of available results, the observation by ASTERIX of a spin 2 resonance at 1565 MeV may well be compatible with the resonance postulated in Ref. [7]. We were therefore led to perform a new high statistics, high precision experiment on the $3\pi^o$ channel.

The $\bar{p}p \rightarrow 3\pi^o$ data were obtained by stopping an external 200 MeV/c antiproton beam from LEAR in the liquid hydrogen target of the Crystal BARrel Detector (CBAR). A detailed description of the CBAR will appear elsewhere [9]. Suffice it to say here that the CBAR is a magnetic detector which covers nearly the full solid angle and is sensitive to both charged particles and photons (Fig. 1). Charged particles coming from annihilations which have occurred in the vicinity of the geometrical centre of the detector are observed and measured in a cylindrical jet drift chamber (JDC). Photons, mainly produced in decays of $\pi^o \rightarrow 2\gamma$, $\eta \rightarrow 2\gamma$, $\omega \rightarrow \pi^o\gamma \rightarrow 3\gamma$, etc. are measured in the electromagnetic CsI calorimeter which surrounds the drift chamber.

As the results presented here depend primarily upon the performance of the electromagnetic calorimeter, we briefly describe its relevant characteristics. The calorimeter consists of 1380 CsI crystals, each 16 radiation lengths in depth; it covers polar angles between 12° and 168°

and has complete coverage in azimuth. Due to the possibility of energy leakage from edge crystals, we limit our polar angle acceptance for e.m. showers to the range between 18° and 162°. This gives a fiducial acceptance for shower detection of 95% of 4π solid angle. At present, the calibration of the crystals is achieved using minimum ionizing particles traversing the whole length of each crystal. The energy resolution is 2.8% for 1 GeV photons and the angular resolution for isolated showers is 20 mrad. The quality of the data is demonstrated in Fig. 2 which shows the two-photon invariant mass spectrum extracted from the six photon event sample used below.

The excellent beam conditions provided by LEAR, and the geometrical and kinematical selections applied to the data guarantee that nearly all the proton antiproton annihilations used in this experiment occur at rest and in liquid hydrogen. This has important consequences for the analysis since it is well known that these annihilations have a limited number of possible initial quantum states.

The incident antiproton trigger is provided by a silicon beam counter placed in the hydrogen target cryostat . Charged final states are vetoed by the JDC. This permits an increase in the data acquisition rate for annihilations into neutral particles (or "0 prong", i.e. 0p) since these represent only 4% of all annihilations. Using a beam with an intensity of 10^4 $\bar{p}$/s, 1.2×10^6 0p events have been accumulated*). This represents the starting sample for the analysis of the reaction:

$$\bar{p}_o p \rightarrow 3\pi^o \qquad (1)$$

(the notation $\bar{p}_o p$ is used for "antiproton-proton annihilations at rest").

Ideally, reaction (1) should correspond in the detector to 0p events with six and only six well defined electromagnetic (e.m.) showers satisfying the energy-momentum relations:

$$\sum_i E_i = 2\, m_p$$

$$\sum_i \vec{p}_i = 0\,, \qquad (2)$$

the sums being extended over all showers with energy E_i and momentum $\vec{p}_i$. An e.m. shower is defined as a signal with more than 20 MeV energy in either one isolated or several

*) This represents the 1989 data. A further 12×10^6 0p events have been obtained in 1990.

neighbouring crystals. Note that two partially overlapping e.m. showers can still be identified as long as two separate energy maxima can be found (the second maximum in this case must be at least 20 MeV).

A Monte Carlo simulation of reaction (1), assuming simply three-body phase space and using GEANT [10] to model the detector and the e.m. shower development, shows that 44% of the events effectively produce six well identified e.m. showers as defined above, and also satisfy the approximate energy-momentum conservation conditions:

$$\left| \sum_i \vec{p}_i \right| < 200 \text{ MeV}$$

$$1675 \text{ MeV} < \sum_i E_i < 2075 \text{ MeV} . \qquad (3)$$

A total of 145,700 events with six e.m. showers survived the cuts given in (3). However, one photon can manifest itself, by e.m. shower fluctuations, as two separated e.m. showers in the detector: the probability depends, of course, on the algorithm which has been used to define an e.m. shower, since the "splinter" (i.e. the second shower maximum) will normally be of low energy (close to our threshold E_{min} = 20 MeV) and close in space to the "parent" (i.e. the main shower component). The combination of the loss of one e.m. shower by the E_{min} cut and the gain of one e.m. shower by the splitting of one photon can result in the creation of six e.m.shower events which may still satisfy the approximate conditions (3) but do not correspond to a real "six photon" final state.

Kinematic fits were therefore applied to isolate the real six photon events corresponding to reaction (1). Firstly, a 4C fit to

$$\bar{p}_o p \rightarrow 6\gamma \qquad (4)$$

yielded 104,000 events which had a probability larger than 10%. (All probability distributions obtained in this analysis are flat above 5 to 8%, so that a cut at 10% is conservative.)

Secondly, 7C fits were applied to the surviving events to select the reactions,

$$\bar{p}_o p \rightarrow \pi^o\pi^o\pi^o , \qquad (1)$$

$$\bar{p}_o p \rightarrow \eta\pi^o\pi^o \text{ and} \qquad (5)$$

$$\bar{p}_o p \rightarrow \eta\eta\pi^o . \qquad (6)$$

Finally, 6C fits were applied to the events failing the 7C fits to select the reaction:

$$\bar{p}_o p \rightarrow \pi^o\pi^o\gamma\gamma \qquad (7)$$

Note that there are *a priori* 15 possible ways to combine the six photons of reaction (4) to form a $3\pi^o$ final state, and 45 combinations to form (5) or (6). All these combinations were tested but, owing to the good resolution of the calorimeter, the potential combinatorial ambiguities turned out to be quite small.

This kinematic selection (imposing probabilities larger than 10%) yielded 51.4×10^3 events fitting uniquely $\bar{p}_o p \rightarrow 3\pi^o$ (one combinatorial solution), 1.5×10^3 $\bar{p}_o p \rightarrow 3\pi^o$ (two solutions) and 2.4×10^3 fitting both $3\pi^o$ and $\eta\pi^o\pi^o$ or $\eta\eta\pi^o$. The number of events yielding three good $3\pi^o$ solutions (36) is completely negligible. The remaining events are easily interpreted in terms of non $3\pi^o$ final states ($\eta\pi^o\pi^o$, $\eta\eta\pi^o$, $\omega^o\omega^o$, etc.) and in terms of the "photon splitting" effect discussed above.

The two combinatorial solutions obtained for 1.5×10^3 $3\pi^o$ events are in general very close to each other on the Dalitz plot; there is no harm in choosing the solution yielding the best probability. The relative rates of well identified $3\pi^o$, $\eta\pi^o\pi^o$ and $\eta\eta\pi^o$ events, i.e. events yielding a unique 7C fit solution with a probability larger than 10%, allow us to split the ambiguous sample (2.4×10^3 events) into 1.9×10^3 "$3\pi^o$", 260 "$\eta\pi^o\pi^o$" and 240 "$\eta\eta\pi^o$" events.

We see that the background due to $\eta\pi^o\pi^o$ and $\eta\eta\pi^o$ in the $3\pi^o$ sample is negligible and the combinatorial ambiguity easily solved. Summing up, 54.8×10^3 events give a $3\pi^o$ 7C kinematic fit with a probability larger than 10%. Applying the same selection cuts and kinematic constraints to a sample of $3\pi^o$ Monte Carlo events, one finds that the global reconstruction efficiency of our method is 30%. One estimates that the $3\pi^o$ final state represents about 1% of all annihilations. This compares well to the results obtained earlier by Devons et al. [3]: $(0.76 \pm 0.23)\%$.

Before discussing the dynamical properties of the $3\pi^o$ sample, we point out that the detection efficiency is nearly independent of the $3\pi^o$ final state configuration: it varies smoothly over the Dalitz plot, with a maximum deviation from the average efficiency of $\pm 4\%$. These small efficiency variations are taken into account with appropriate weighting in the following analysis.

The Dalitz plot of the $3\pi^o$ final state is shown in Fig. 3a. The most conspicuous feature of this plot is the absence of events at the centre. This effect is explained by the importance of the

initial antiproton-proton P states, which are characterized [11] by a zero in their amplitudes at $|\vec{p}_1| = |\vec{p}_2| = |\vec{p}_3|$ ($\vec{p}_i$: momentum of π^o_i, i = 1,2,3), and, as we shall see below, by a destructive interference effect between the two most important amplitudes related to the ^1S_o initial state. The accumulations observed in the bands at $2\pi^o$ squared mass around 1.60 GeV^2 and in particular at the intersection of these bands are naturally interpreted in terms of the $f_2(1270)$ meson. However, there exists no generally accepted explanation for the other accumulations observed in the regions centred around 2.4 GeV^2 of the $2\pi^o$ mass squared. As we shall see below, introducing two more resonances can account for these accumulations. This qualitative interpretation of the Dalitz plot also provides a natural interpretation of the $2\pi^o$ effective mass spectrum (Fig. 4a), where two peaks are observed around 1300 MeV and 1500 MeV. The observation of $2\pi^o$ resonances in the final state, and in particular the fact that at least one of these seems to correspond to the well established $f_2(1270)$ meson encourages us to analyze the Dalitz plot in terms of $2\pi^o$ final state interactions.

Since the final state ($3\pi^o$) has C = +1 and since only S and P states of $\bar{p}_o p$ have appreciable annihilation probability, the allowed initial states are limited to ^1S_o ($J^{PC} = 0^{-+}$), $^3P_1$ ($J^{PC} = 1^{--}$) and $^3P_2$ ($J^{PC} = 2^{++}$) with total isospin 1.

The invariant transition amplitudes can be written as

$$A_{J\ell} = \sum_{i=1}^{3} F_\ell(q,m)_{jk}\, S_{J,L\ell}(\vec{p},\vec{q})_i, \quad i,j,k = 1,2,3 \tag{8}$$

the sum being extended over the three (2π)-π configurations, in order to satisfy the necessary symmetry. J is the total spin of the initial state; $\vec{p}$ and L are the momentum of the pion recoiling against the dipion and the pion-dipion angular momentum in the $\bar{p}_o p$ rest system, respectively; $\vec{q}$ and ℓ are the momentum and angular momentum in the dipion system. $S_{J,L\ell}(\vec{p},\vec{q})$ are the spin parity functions constructed according to the method developed by Zemach [11] (Table 1), $F_\ell(q,m)$ is a dynamical form factor; m is the dipion invariant mass.

In the following, we assume isospin I = 0 for the $2\pi^o$ system, and limit the analysis to $\ell = 0$ or 2, and $L \leq 2$.

For the $\pi\pi$ S-wave ($\ell = 0$), we assume:

$$F_o(q,m) = \frac{m}{q} e^{i\delta} \sin\delta \tag{9}$$

taking the values of δ from the work of Au, Morgan and Pennington (AMP) [12] which describes well all measurements made on this system from threshold up to ~ 1700 MeV. For the $\pi\pi$ D wave ($\ell = 2$), we first introduce the only well-known $\pi\pi$ spin 2, I = 0 resonance, i.e. the $f_2(1270)$, using the Breit-Wigner function [13].

$$F_2(q, m) = \left(\frac{m}{q}\right)^{1/2} \frac{[\Gamma(m)]^{1/2}}{(m_o^2 - m^2) - i\, m_o \Gamma(m)}, \text{ with } \Gamma(m) = \left(\frac{q}{q_o}\right)^5 \frac{m_o}{m} \Gamma . \qquad (10)$$

The position of the resonance is denoted by m_o, its width by Γ and the value of q at m_o by q_o.

The experimental event density on the Dalitz plot is compared to the Monte Carlo simulated intensity corresponding to the sum:

$$I = I_0 + I_1 + I_2 \quad \text{with}$$

$$I_0 = | a_{00}A_{00} + a_{02}A_{02} |^2 \qquad \text{for the } {}^1S_0 \text{ initial state}$$

$$I_1 = | a_{10}A_{10} + a_{12}A_{12} |^2 \qquad \text{for the } {}^3P_1 \text{ initial state} \qquad (11)$$

$$I_2 = | a_{22}A_{22} |^2 \qquad \text{for the } {}^3P_2 \text{ initial state} .$$

Here, $a_{J\ell}$ are complex parameters; their magnitudes and relative (not absolute) phases are measurable for each specific initial state. The normalization of the amplitudes $A_{J\ell}$ is such that the integration of each $|A_{J\ell}|^2$ over the Dalitz plot is equal to the total number of events. The adjustment of the free parameters (the $a_{J\ell}$ of eq. 11) is made on one sextant of the Dalitz plot which has been divided into 561 bins.

Introducing these five basic amplitudes does not yield a good interpretation of the data ($\chi^2/N_{dof} = 5038/554$) and leaves unexplained the enhancement observed at ~ 1515 MeV in the $\pi^o\pi^o$ effective mass spectrum. We therefore introduce three additional amplitudes for the production of a state centred at 1515 MeV from the three possible initial states, representing this state by the Breit-Wigner function (10) for spin 2 or by a similar function but with

$$\Gamma(m) = \frac{q}{q_o} \frac{m_o}{m} \Gamma$$

for spin 0. The fit over the Dalitz plot improves considerably, in particular for spin 2: χ^2/N_{dof} = 1983/548, and χ^2/N_{bin} = 270/50 in the 1515 MeV $2\pi^o$ mass window A (see Fig. 3b), whereas for spin 0, χ^2/N_{bin} = 426/50. However, it leaves unexplained a significant excess of events at large $\pi^o\pi^o$ invariant masses. This excess cannot be reduced by varying the mass and the width of the 1515 MeV state. One finds instead that its origin must be sought in a $\pi^o\pi^o$ D wave from the $^3P_2$ $\bar{p}_o p$ initial state. We therefore add a third spin 2 $\pi\pi$ resonance:

$$A_{02} = \sum_{i=1}^{3} [F_2(q, 1270) + c_{01} F(q, 1515)]_{j,k} S_{0,22}(\vec{p}, \vec{q})_i$$

$$A_{12} = \sum_{i=1}^{3} [F_2(q, 1270) + c_{11} F(q, 1515)]_{j,k} S_{1,12}(\vec{p}, \vec{q})_i \qquad (12)$$

$$A_{22} = \sum_{i=1}^{3} \left[F_2(q, 1270) + c_{21} F_2(q, 1515) + c_{22} F_2(q, 1810)\right]_{j,k} S_{2,12}(\vec{p}, \vec{q})_i,$$

where c_{J1} and c_{J2} are complex parameters. In this formula we have introduced the $f_2(1810)$ as the most likely candidate [14] for the highest mass resonance.

We now get an excellent representation of the observations, in particular in the high $2\pi^o$ mass region. The fit is not too sensitive to the mass and width used for the $f_2(1810)$, which can be taken in the range M = 1790 ± 50 MeV and Γ = 250 ± 100 MeV without significantly changing the results. The masses and widths used in the fit for the $f_2(1270)$ and $X_2(1515)$ are the mean values derived from the data by χ^2 fits on the Dalitz plot, iterating the masses and widths, yielding the values:

$f_2(1270)$: M = 1275 ± 10 MeV , Γ = 200 ± 10 MeV

$X_2(1515)$: M = 1515 ± 10 MeV , Γ = 120 ± 10 MeV .

We note that the results of the fit do not depend on the initial values of the free parameters. The χ^2 over the Dalitz plot is: χ^2/N_{dof} = 693/546 and, in the $2\pi^o$ mass window A (see Fig. 3b): χ^2/N_{bin} = 79/50. In contrast, spin 0 for the 1515 MeV resonance gives over the Dalitz plot χ^2/N_{dof} = 1048/548 and in the $2\pi^o$ mass window A: χ^2/N_{bin} = 265/50. Of the nine amplitudes introduced in this complete fit: $\pi^o\pi^o$ S wave, $f_2(1270)$ and $X_2(1515)$ from ^1S_o and $^3P_1$, $f_2(1270)$, $X_2(1515)$ and $f_2(1810)$ from $^3P_2$, two come out with a non-significant contribution: (0.8 ± 0.2)% for $\pi^o\pi^o$ S wave from $^3P_1$ and (0.0 ± 0.1)% for $f_2(1270)$ from $^3P_2$. We therefore repeat the analysis keeping only the seven amplitudes which contribute significantly to the $3\pi^o$

final state. The quality of this final fit is comparable to the fit tried above with nine amplitudes: χ^2/N_{dof} = 722/550 over the Dalitz plot with χ^2/N_{bin} = 67/50 in the $2\pi^o$ mass window A for $X_2(1515)$. Figure 3b shows the bins in the Dalitz plot which contribute most to the χ^2 obtained for this best fit. We exclude a spin 0 interpretation of the X(1515) since repetition of the final fit with this hypothesis gives a much worse χ^2 (χ^2/N_{dof} = 1331/552). Similarly, we favour a resonance interpretation since repetition of the final fit where the complex Breit-Wigner amplitude is replaced by a similar scalar form factor for spin 2 again gives a much worse χ^2 (χ^2/N_{dof} = 1719/553). The quality of the fit is further illustrated in Fig. 4 (a-d).

We thus conclude that the $\pi^o\pi^o$ enhancement observed at 1515 MeV is a resonance, with:

$$I = 0 \text{ or } 2\,, \quad J^{PC} = 2^{++}\,, \quad M = 1515 \pm 10 \text{ MeV} \quad \Gamma = 120 \pm 10 \text{ MeV}\,.$$

The final results are given in Table 2. In this table, we quote statistical and systematic errors. The former come from the fit itself [15]: they are checked by repeating the fit on four independent subsets of the data and by comparing the quoted statistical errors to the dispersion obtained in this way. The systematic errors include the effect of varying the event selection criteria (minimum permitted photon energy and the minimum probability required for the kinematic fits) and the parameters entering in the fit (masses and widths of all resonances, effect of excluding negligible amplitudes). One sees that ~ 60% of $3\pi^o$ annihilations originate from P states, which is to be compared to the 8.5% measured by Doser et al. [16] for all $\bar{p}_o p$ annihilations in liquid hydrogen. The two numbers are consistent if the branching ratio for $3\pi^o$ production from P states is larger by a factor of about 7 than from S states. About 30% of the $3\pi^o$ are associated with the $\pi^o\pi^o$ S wave (using the AMP parametrization), and the rest with the $\pi^o\pi^o$ D wave: ~ 22% are associated with the $f_2(1270)$, ~ 26% with the $X_2(1515)$, and ~ 23% with a higher mass resonance at ~ 1800 MeV. Note that no direct three-body decay amplitudes have been introduced in the final fit.

We may compare our $X_2(1515)$ resonance with the 2π phenomena previously observed in the 1500-1600 MeV region in 3π annihilations. In view of the dominance of the $\rho(770)$ intermediate resonance in the $\pi^+\pi^-\pi^o$ channel, especially originating from initial S states, it is understandable that Foster et al. [1] did not notice any resonance in the relevant region. Presumably for the same reason, May et al. [8] could not detect it in their data on the annihilations from pure S states. The higher mass (1565 ± 20) MeV and the larger width (170 ± 40) MeV observed by May et al. [8] in their analysis of annihilations from pure P states is probably again due to the strong $\rho(770)$ excitation which prevented the resolution of the high mass enhancement into two resonances at 1515 and 1810 MeV, as suggested by our experiment. Within errors, $X_2(1515)$ is perfectly compatible with the resonance at 1527 MeV of Gray et al. [7] except, of course, for the spin assignment. Note that both Gray et al. and May

et al. could exclude I = 2 for the new resonance since it is not present in the charged 2π combinations.

It is intriguing that the $X_2(1515)$ is presently uniquely associated with antiproton-nucleon annihilations. Of course, we cannot completely exclude the possibility that the phenomenon attributed to $X_2(1515)$ is an artefact of antinucleon-nucleon annihilation dynamics. However, a resonating form factor as postulated here and in [7] and [8] seems the most economical hypothesis capable of describing the reaction. The latter argument and the systematics of resonance production in antinucleon-nucleon annihilations [17] also speak in favour of explaining the intensity in the corners of the Dalitz plot of Fig. 3a by a high mass resonance such as the $f_2(1810)$.

The $X_2(1515)$ cannot be identified with the well-established $s\bar{s}$ f_2' (1525) meson because this assumption would imply a production of f_2' (1525) two orders of magnitude larger than the upper limit found from the analysis of $\bar{p}_o p \to K_s^o K_s^o \pi^o$ [18]. The same observation has been made before by Gray et al. [7]. We are thus led to postulate the existence of two states with the same $I^G(J^{PC})$ quantum numbers and similar masses and widths. A selection rule (e.g. the OZI selection rule) could prevent them from mixing to an appreciable degree. Interestingly though, even if they mix strongly, their properties could turn out as observed [19]. In this latter case, it may prove difficult to unveil the properties of the two original states. The experimental study of the two states in as many combinations of entrance and exit channels as possible might facilitate this task.

We refrain from speculating on the fundamental nature of the two states around 1520 MeV. Instead, we refer to a recent paper [20] where a case for a quasi-nuclear bound state interpretation of one of them has been made but other possibilities are also discussed.

Acknowledgements

We would like to thank the technical staff of the LEAR machine group and of all the participating institutions for their invaluable contributions to the success of the experiment. We acknowledge financial support from the German Bundesministerium für Forschung und Technologie, the Schweizerische Nationalfonds, the British Science and Engineering Research Council and the U.S. Department of Energy (contract No. DE-FG03-87ER40323 and DE-AC03-76SF00098). K.K. acknowledges support from the Heisenberg Foundation.

REFERENCES

[1] M. Foster et al., N.P. B6 (1968) 107.

[2] P. Anninos et al., P.R.L. 20 (1968) 402.

[3] S. Devons et al., P.L. B47 (1973) 271.

[4] G. Veneziano, N.C. 57A (1968) 190.
C. Lovelace, P.L. 28B (1968) 264.
G. Altarelli and H. Rubinstein, P.R. 183 (1969) 1469
E.M. Levin, Sov. Phys. Usp. 16 (1974) 600.

[5] A. Nandy, P.H. Frampton, T.E. Kalogeropoulos, P.R. D11 (1975) 1040.
T.E. Kalogeropoulos et al., P.R. D24 (1981) 1759.

[6] P.H. Kasper, G.I. Opat, D.D. Carmony, Univ. of Melbourne Report, 1981 (unpublished).

[7] L. Gray et al., P.R. D27 (1983) 307.

[8] B. May et al., P.L. 225 B (1989) 450, and ZPHY. C46 (1990) 191; C46 (1990) 203.

[9] E. Aker et al., The Crystal Barrel Collaboration, in preparation.

[10] R. Brun et al., GEANT 3, CERN-DD/EE/84-1, 1987.

[11] Ch. Zemach, P.R. B 133 (1964) 1201; P.R. B 140 (1965) 97, 109.

[12] K.L. Au, D. Morgan, M.R. Pennington, P.R. D 35 (1987) 1633.

[13] G. Breit and E. Wigner, P.R. 49 (1936) 519.
D. Jackson, N.C. 34 (1964) 1644.

[14] Review of Particle Properties (PDG), P.L. 239 (1990) 1.

[15] F. James and M. Roos, Comp. Physics Com. 10 (1975) 10.

[16] M. Doser et al., N.P. A 486 (1988) 493.

[17] J. Vandermeulen, Z.P. C37 (1988) 563.

[18] B. Conforto et al., N.P. B3 (1967) 469.

[19] J.F. Donoghue, P.R. D25 (1982) 1875.

[20] C.B. Dover et al., BNL 44829, June 1990, and P.R.C. (in press).

Table 1

Zemach spin-parity functions for $\bar{p}p \rightarrow 3\pi^o$

Initial state	ℓ, L	$S_{J,L\ell}$
^1S_o	0, 0	1
	2, 2	$(\vec{q}_i \bullet \vec{p}_i)^2 - \frac{1}{3} \mid \vec{q}_i \mid^2 \mid \vec{p}_i \mid^2$
$^3P_1$	0, 1	$\vec{p}_i$
	2, 1	$\vec{q}_i(\vec{q}_i \bullet \vec{p}_i) - \frac{1}{3} \mid \vec{q}_i \mid^2 \vec{p}_i$
$^3P_2$	2, 1	$\frac{1}{2}[\vec{q}_j \otimes (\vec{q}_j \times \vec{p}_j) - \vec{q}_k \otimes (\vec{q}_k \times \vec{p}_k)]$

Table 2

Results of the final fit

Initial state	Intermediate final state			
	Amplitude ($a = \alpha e^{i\phi}$)		Fraction %	Total %
$^1S_o(0^{-+})$	$\pi^o\pi^o$ S wave	$\alpha_1 = 0.549\pm0.027\pm0.010$	28.3±1.8±1.7	
	$f_2(1270)$	$\alpha_2 = 0.163\pm0.014\pm0.034$	2.9 ±0.5±1.0	40.7±1.2
	$X_2(1515)$	$\alpha_3 = 0.302\pm0.013\pm0.019$	9.5 ±0.2±0.7	±1.7
		$\phi_{12} = 0.71 \pm0.09 \pm0.22$		
		$\phi_{13} = 2.93 \pm 0.08\pm0.24$		
$^3P_1(1^{++})$	$f_2(1270)$	$\alpha_4 = 0.601\pm0.009\pm0.062$	19.3±0.9±0.7	
	$X_2(1515)$	$\alpha_5 = 0.387\pm0.014\pm0.035$	8.0±0.4±0.3	27.3±1.3
		$\phi_{45} = 4.58 \pm0.09 \pm0.30$		±0.8
$^3P_2(2^{++})$	$X_2(1515)$	$\alpha_6 = 0.305\pm0.064\pm0.023$	8.8±0.9±0.7	
	$f_2(1810)$	$\alpha_7 = 0.496\pm0.016\pm0.082$	23.2±2.1±4.1	32.0±1.3
		$\phi_{67} = 2.46 \pm0.28 \pm0.86$		±0.7

Figure captions

Fig. 1 : Sketch of the Crystal Barrel detector. (The magnet and the incident antiproton trigger counters are not shown.)

Fig. 2 : The invariant two photon effective mass spectrum extracted from the six photon event sample (15 combinations per event): one clearly sees π^o and η peaks. The upper inset shows the $\gamma\gamma$ invariant mass distribution of those $\gamma\gamma$ pairs which do not contribute to the π^o mass window; the combinatorial background is reduced and the η signal becomes more apparent. If the η mass window is also excluded, the $\eta' \rightarrow \gamma\gamma$ decay can be seen (lower inset). The peak at 770 MeV is due to $\pi^o\pi^o\omega$ events with $\omega^o \rightarrow \pi^o\gamma$ where one very low energy γ was unobserved.

Fig. 3 : a) $3\pi^o$ Dalitz plot. Each event is plotted six times, once in each of the six sextants. b) the same $3\pi^o$ Dalitz plot. The mass windows A and B as defined on this figure are used to study the quality of fits in the X(1515) mass region and along a diagonal of the Dalitz plot. The dark grey cells in the upper left (right) sextant indicate the cells where the value of the density obtained with the final fit is smaller (larger) than the experimental value ($\chi^2 > 4$).

Fig. 4 : a) $\pi^o\pi^o$ effective mass spectrum. The peaks corresponding to the $f_2(1270)$ and $X_2(1515)$ are dominant at high mass. The enhancements at low mass are due to a combination of the $\pi^o\pi^o$ S wave and of the reflections of high mass resonances. The continuous line shows the projection of the final fit [including an X(1515) with J = 2]. The dashed line shows the projection of a fit including an X(1515) but with J = 0. The dotted line shows the projection of a fit without any X(1515). The mixed line shows the contribution of the $\pi^o\pi^o$ S wave in the final fit.

b) Decay angular distribution of the X(1515) corresponding to the events in window A of Fig. 3b. The continuous line shows the projection of the final fit [with J = 2 for the X(1515)]. The dashed line shows the projection of the fit assuming J = 0 for the X(1515). The slight irregularities in the curves are due to the limited Monte Carlo statistics used in the fit.

c) Decay angular distribution of the $f_2(1270)$. Definition of the curves as in Fig. 4b.

d) Distribution of data along a Dalitz plot diagonal (window B of Fig. 3b): the $X_2(1515)$ shows up clearly with a lopsided shape due to the $f_2(1810)$. The minimum around 1 GeV/c^2 corresponds to the hole observed at the Dalitz plot centre. The enhancement at low mass is mainly due to the interfering $f_2(1270)$ amplitudes. Definition of the curves as in Fig. 4c.

Crystal Barrel Detector

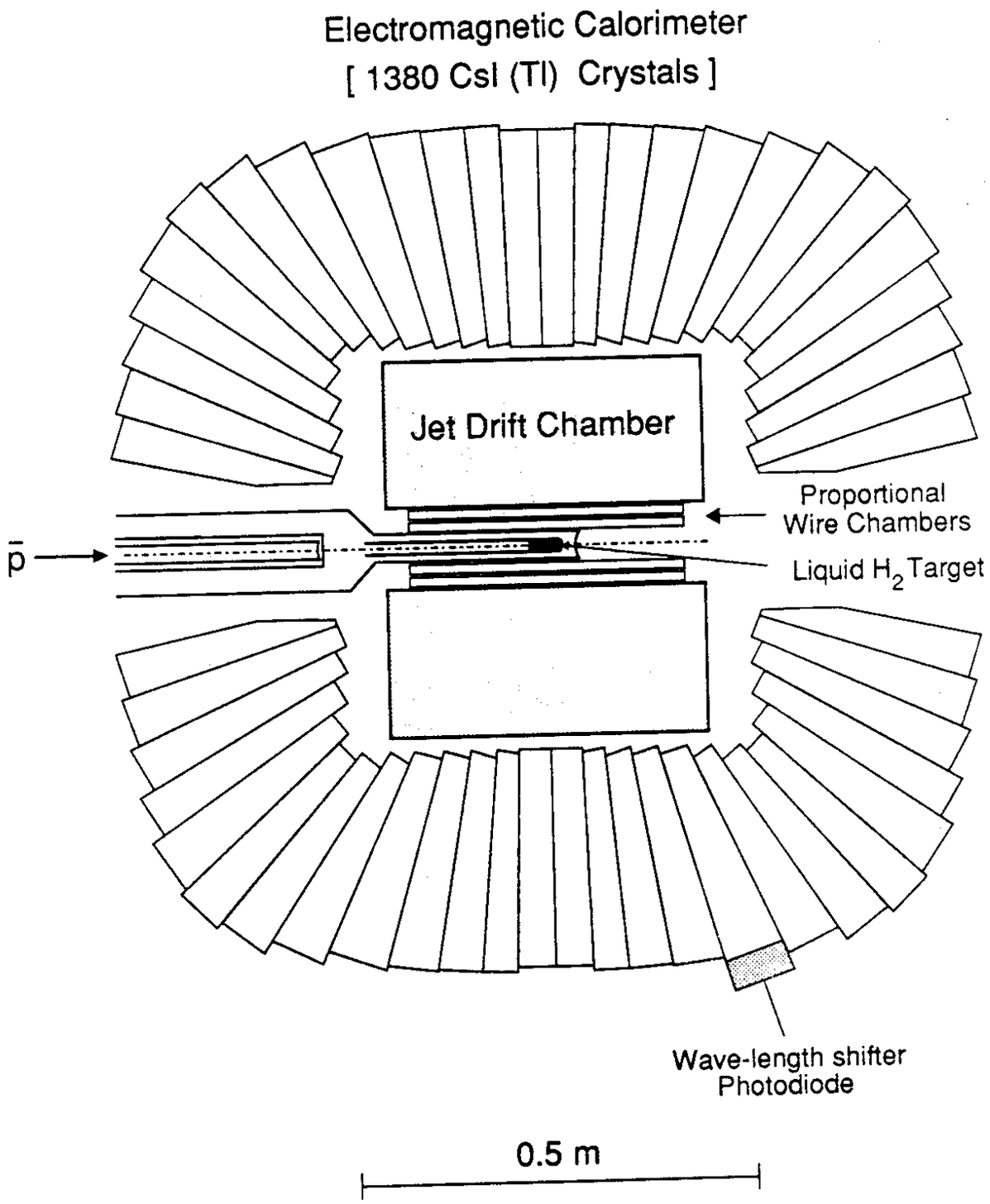

FIG. 1

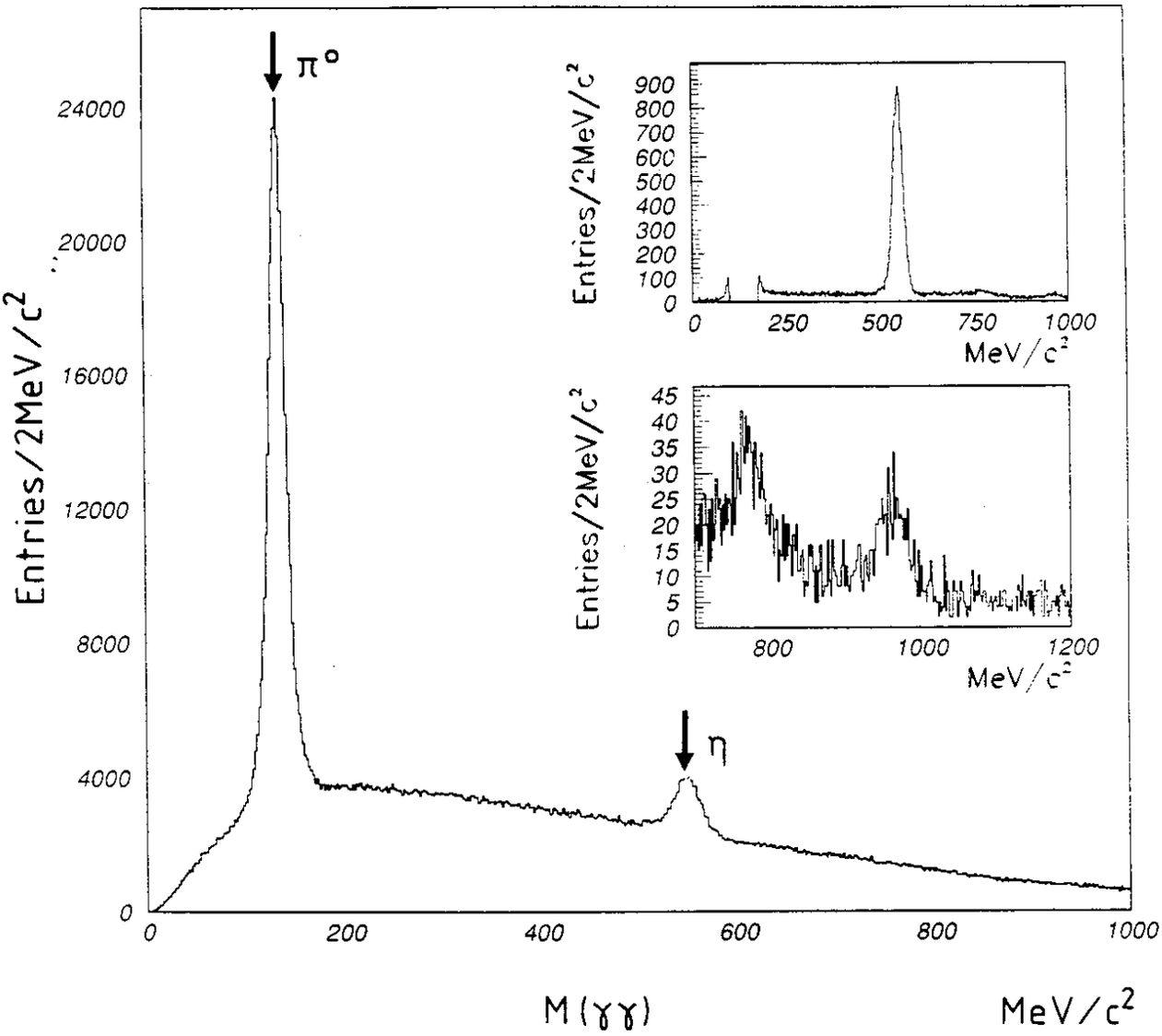
π°
η
Entries/2MeV/c²
24000
20000
16000
12000
8000
4000
0
0
200
400
600
800
1000
M(γγ)
MeV/c²
Entries/2MeV/c²
900
800
700
600
500
400
300
200
100
0
0
250
500
750
1000
MeV/c²
Entries/2MeV/c²
45
40
35
30
25
20
15
10
5
0
800
1000
1200
MeV/c²

Fig. 2

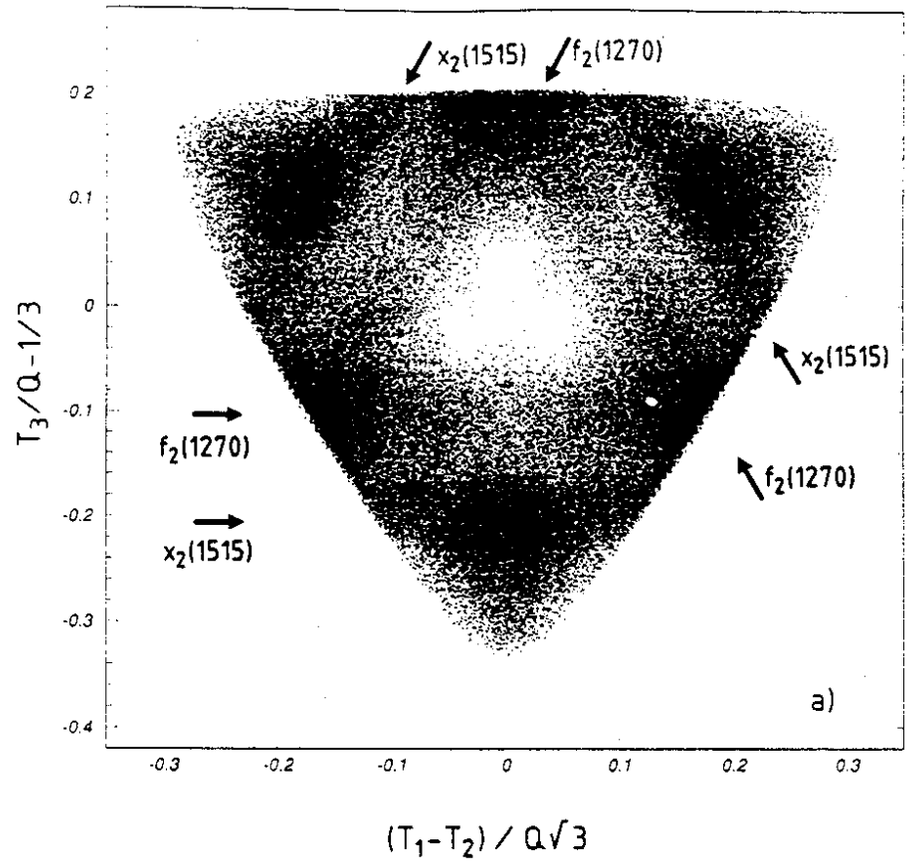
x2(1515)
f2(1270)
x2(1515)
f2(1270)
f2(1270)
x2(1515)
a)
T3/Q-1/3
(T1-T2) / Q√3

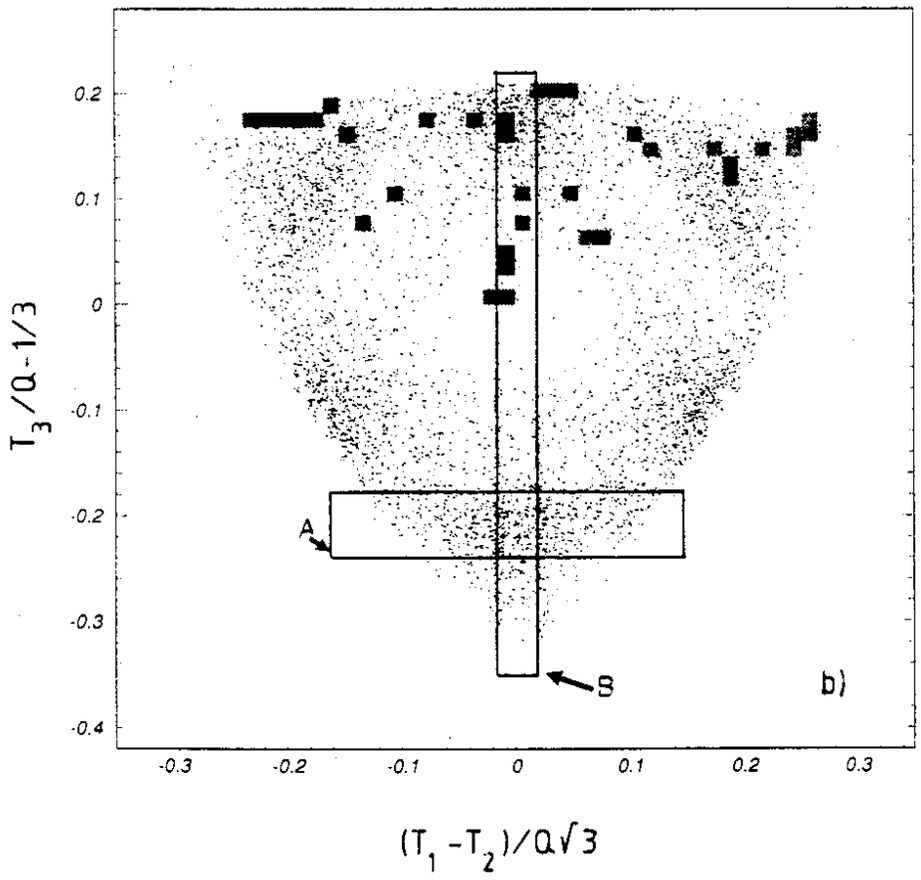
A
B
b)
T3/Q-1/3
(T1-T2)/Q√3

Fig. 3

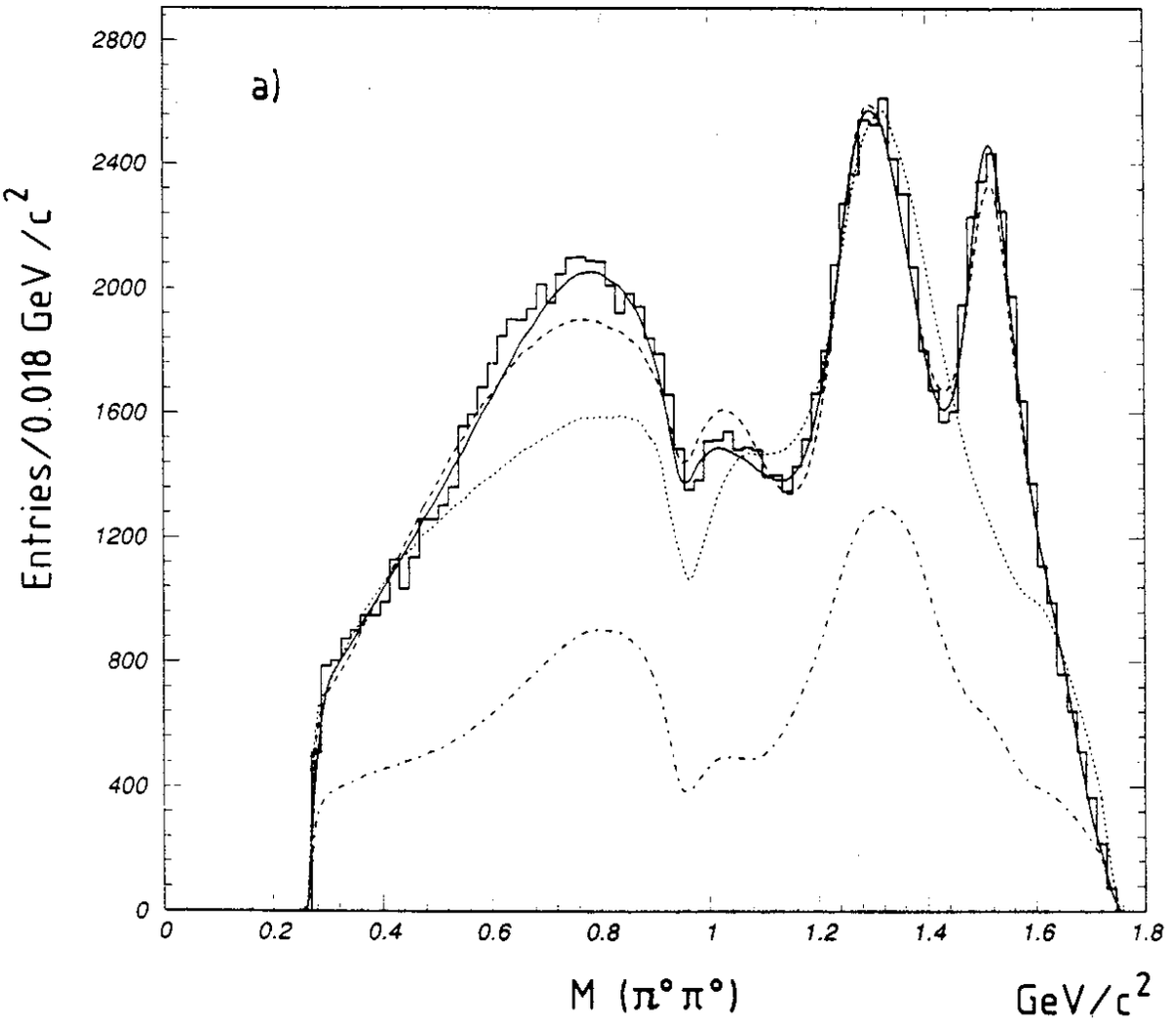
a)
Entries/0.018 GeV/c^2
2800
2400
2000
1600
1200
800
400
0
0
0.2
0.4
0.6
0.8
1
1.2
1.4
1.6
1.8
M ($\pi^\circ\pi^\circ$)
GeV/c^2

Fig. 4a)

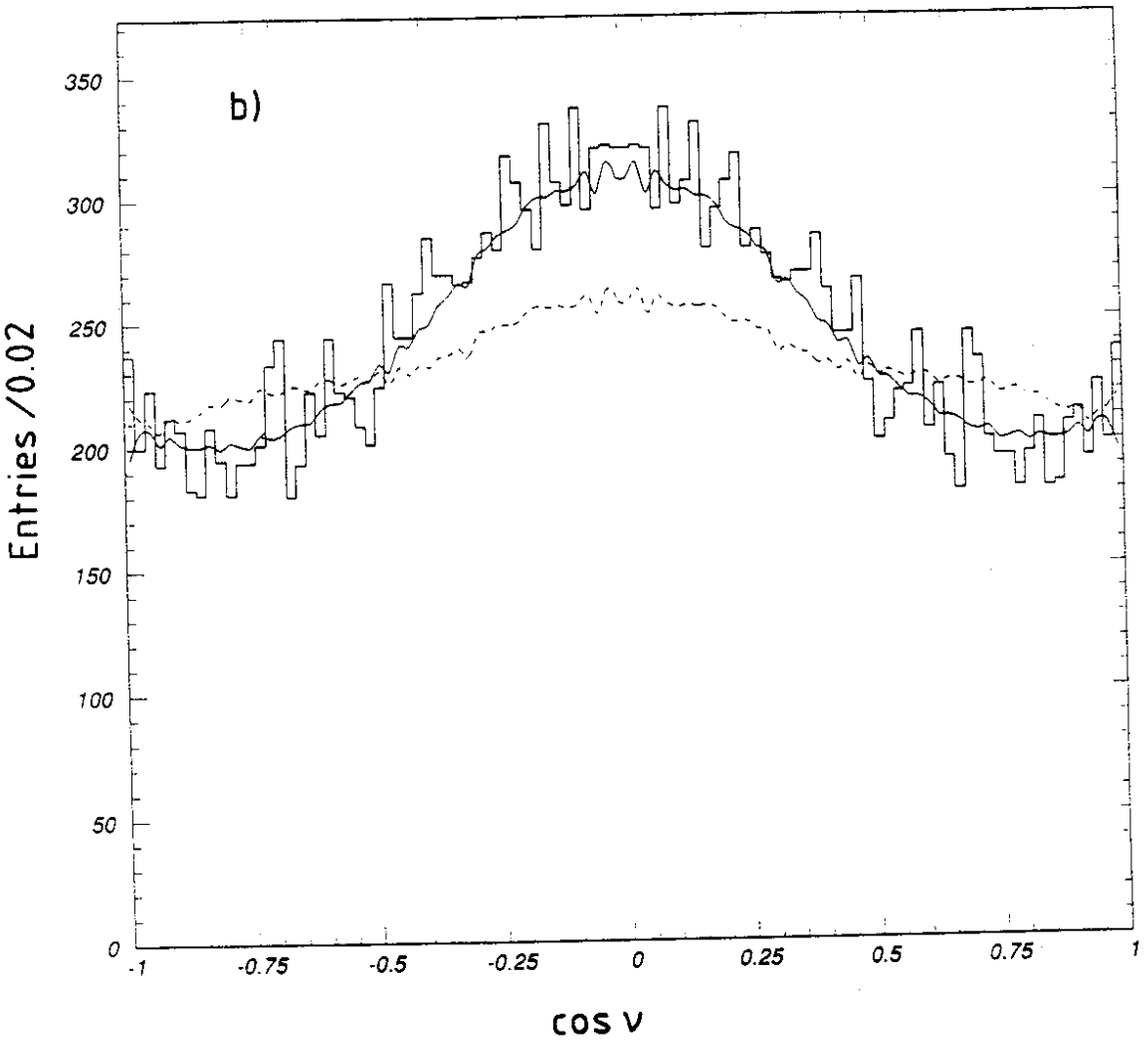
b)
Entries /0.02
350
300
250
200
150
100
50
0
-1
-0.75
-0.5
-0.25
0
0.25
0.5
0.75
1
cos ν

Fig. 4b)

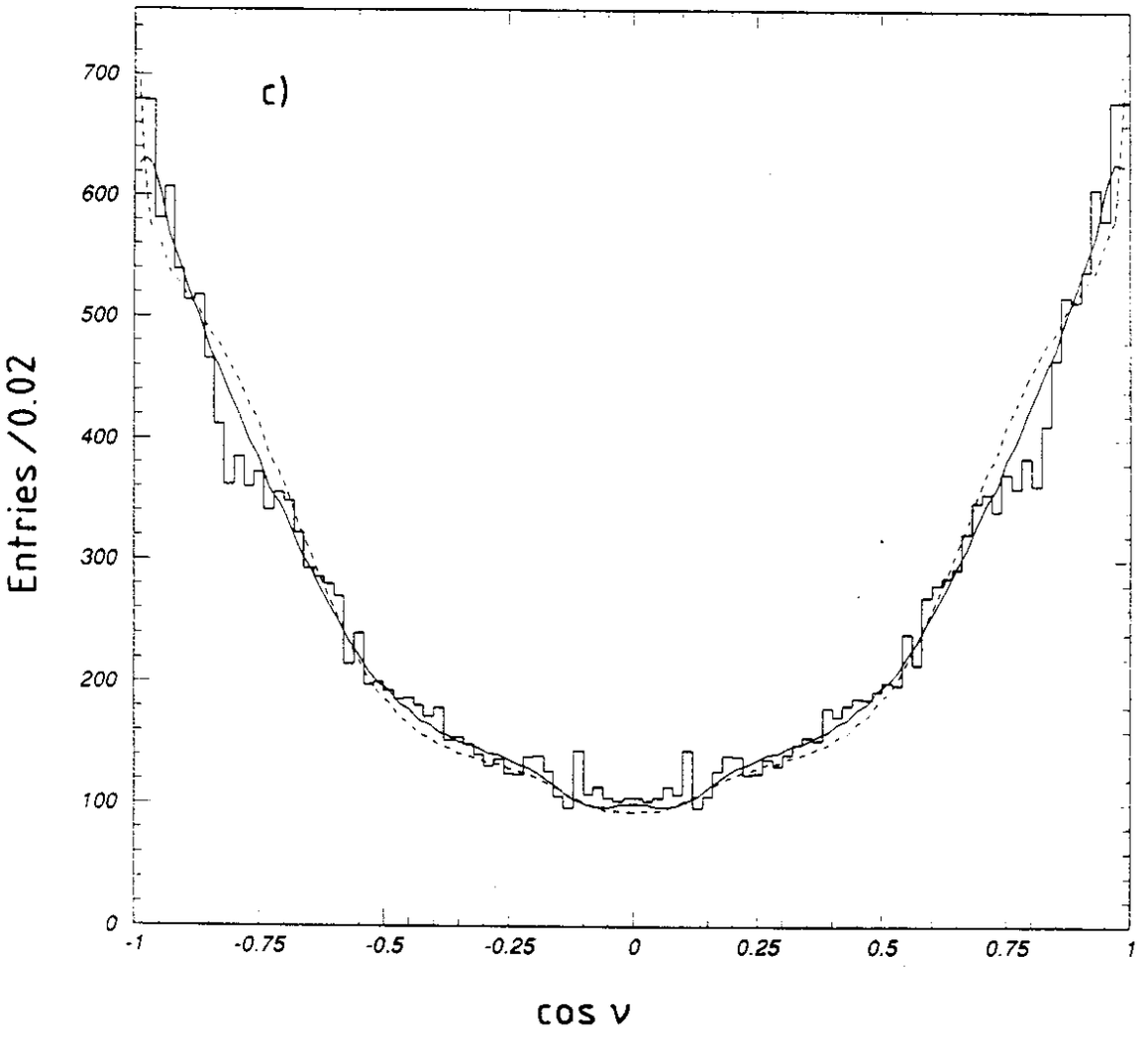
c)
Entries /0.02
700
600
500
400
300
200
100
0
-1
-0.75
-0.5
-0.25
0
0.25
0.5
0.75
1
cos ν

Fig. 4c)

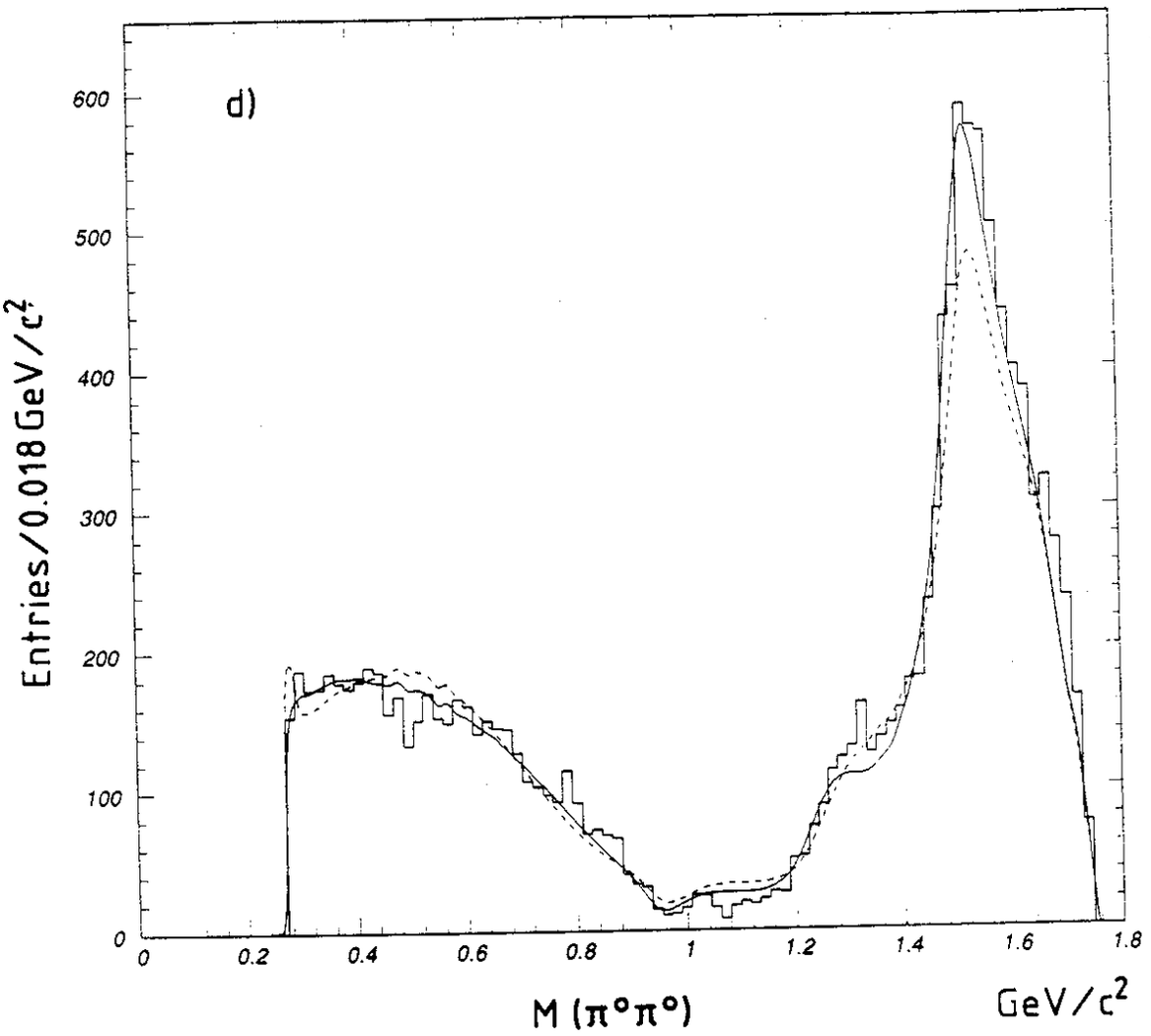
d)
Entries/0.018 GeV/c²
M (π°π°)
GeV/c²
0
100
200
300
400
500
600
0.2
0.4
0.6
0.8
1
1.2
1.4
1.6
1.8

Fig. 4d)